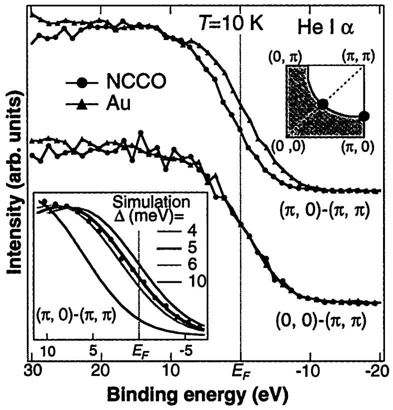

Fig. 3. Angle-resolved photoemission spectra near E_F of $Nd_{2-x}Ce_xCuO_4$ (x = 0.15, T_c = 22 K) measured at 10 K at the (π,0)-(π,π) and the (0,0)-(π,π) crossing, compared with the gold reference measured under the same condition. Inset shows the result of numerical fitting with various gap values.

binding energy relative to that of the gold spectrum, indicating that a superconducting gap opens in this direction. In contrast, the leading edge of ARPES spectrum at the (0,0)-(π,π) crossing almost coincides with the gold reference, suggesting no superconducting gap or a very small one. These spectral behaviors are qualitatively the same as those of BSCCO (*12*, *13*), which have established an anisotropic superconducting gap in the hole-doped HTSC. Thus, the present ultrahigh-resolution ARPES clearly shows that an anisotropic superconducting gap opens also in the electron-doped HTSC. Although a possibility of an anisotropic *s* symmetry with a very small gap at the (0,0)-(π,π) crossing is not excluded because of the finite energy resolution, we conclude that the most probable symmetry deduced from the present result is $d_{x^2-y^2}$ as in the hole-doped HTSCs (*12*, *13*).

We now discuss the size of superconducting gap (Δ) in NCCO. The shift of the leading edge of ARPES spectrum at the (π,0)-(π,π) crossing is about 2 to 3 meV, but it is noted that this value is not equal to the Δ itself because of the finite energy resolution and the thermal broadening. According to the ARPES result on BSSCO (*26*), the gap size is found to be almost twice that of the leading-edge shift. When applied to the NCCO case, we obtain a gap value of 4 to 6 meV. In order to estimate the gap size more quantitatively, we fitted the spectrum by the BCS (Bardeen-Cooper-Schrieffer) spectral function with broadening of 0.1 meV, multiplied by the Fermi-Dirac function and convoluted with the energy resolution, as has been employed in the hole-doped HTSCs (*26*). We found that the leading edge of ARPES spectrum is relatively well fitted, whereas the higher binding-energy part is not so satisfactorily reproduced. This may be due to the incoherent part of the spectral function and the inelastically scattered secondary electrons, which are not accounted in the simulation. The inset to Fig. 3 shows the result of simulation near E_F. The simulation curve with a 10-meV gap, which corresponds to $2\Delta/k_BT_c \sim 10$ as in the optimally doped BSCCO (*26–28*), does not fit the experimental result. This suggests that the superconducting gap of NCCO is much smaller than 10 meV, and, as a result, the $2\Delta/k_BT_c$ value is also smaller than that of BSCCO. Simulations with $\Delta = 5 \pm 1$ meV fit the experimental curve relatively well. This result seems consistent with the tunneling experiments that have proposed the Δ being about 4 meV (*2*, *6*, *9*). The $2\Delta/k_BT_c$ value of NCCO is thus nearly half that (8-10) of optimally doped BSCCO (*26–28*), but both have the $d_{x^2-y^2}$–like superconducting order parameter. Although this difference may be related to the difference in the details of the electronic structure near E_F such as the position of the van Hove singularity, we leave this as a challenge for theory.

References and Notes

1. R. D. Parks, *Superconductivity* (Dekker, New York, 1969).
2. Q. Huang *et al.*, *Nature* **347**, 369 (1990).
3. D. H. Wu *et al.*, *Phys. Rev. Lett.* **72**, 85 (1993).
4. A. Andreone *et al.*, *Phys. Rev. B* **49**, 6392 (1996).
5. Y. Tokura, H. Takagi, S. Uchida, *Nature* **337**, 345 (1989).
6. F. Hayashi, E. Ueda, M. Sato, K. Kurahashi, K. Yamada, *J. Phys. Soc. Jpn.* **67**, 3234 (1998).
7. C. C. Tsuei, J. R. Kirtley, *Phys. Rev. Lett.* **85**, 185 (2000).
8. J. D. Kokales *et al.*, *Phys. Rev. Lett.* **85**, 3696 (2000).
9. R. Prozorov, R. W. Giannetta, P. Fournier, R. L. Greene, *Phys. Rev. Lett.* **85**, 3700 (2000).
10. L. Alff *et al.*, *Phys. Rev. Lett.* **83**, 2644 (1999).
11. S. Kashiwaya *et al.*, *Phys. Rev. B* **57**, 8680 (1998).
12. Z.-X. Shen *et al.*, *Phys. Rev. Lett.* **70**, 1553 (1993).
13. H. Ding *et al.*, *Phys. Rev. B* **54**, R9678 (1996).
14. After the completion of this work, we became aware of ARPES work by N. P. Armitage *et al.* [e-Print available at http://xxx.lanl.gov/abs/cond-mat/0012003], which comes to essentially the same conclusion.
15. Because the surface degradation was remarkably enhanced at higher temperatures, we could not obtain reliable data at higher temperatures.
16. Y. Sakisaka *et al.*, *Phys. Rev. B* **42**, 4189 (1990).
17. O. Gunnarsson, O. Jepsen, Z.-X. Shen, *Phys. Rev. B* **42**, 8707 (1990).
18. R. O. Anderson *et al.*, *Phys. Rev. Lett.* **70**, 3163 (1993).
19. H. M. Fretwell *et al.*, *Phys. Rev. Lett.* **84**, 4449 (2000).
20. S. V. Borisenko *et al.*, *Phys. Rev. Lett* **84**, 4453 (2000).
21. D. M. King *et al.*, *Phys. Rev. Lett.* **73**, 3298 (1994).
22. T. Valla *et al.*, *Science* **285**, 2110 (1999).
23. A. Kaminski *et al.*, *Phys. Rev. Lett.* **84**, 1788 (2000).
24. P. V. Bogdanov *et al.*, *Phys. Rev. Lett.* **85**, 2583 (2000).
25. M. R. Norman *et al.*, *Phys. Rev. Lett.* **79**, 3506 (1997).
26. H. Ding *et al.*, *Phys. Rev. Lett.* **74**, 2784 (1995).
27. A. V. Fedorov *et al.*, *Phys. Rev. Lett.* **82**, 2179 (1999).
28. J. Mesot *et al.*, *Phys. Rev. Lett.* **83**, 840 (1999).
29. M. R. Norman *et al.*, *Nature* **392**, 157 (1998).
30. Supported by grants from the CREST (Core Research for Evolutional Science and Technology) Corporation of JST, the Japan Society for Promotion of Science (JSPS), and the Ministry of Education, Science and Culture of Japan. T.S. thanks the JSPS for financial support.

5 December 2000; accepted 13 January 2001

Rapid Electron Tunneling Through Oligophenylenevinylene Bridges

Hadley D. Sikes,[1] John F. Smalley,[2]* Stephen P. Dudek,[1]
Andrew R. Cook,[2] Marshall D. Newton,[2]*
Christopher E. D. Chidsey,[1]* Stephen W. Feldberg[2]*

We measured rate constants of thermal, interfacial electron transfer through oligophenylenevinylene bridges between a gold electrode and a tethered redox species in contact with an aqueous electrolyte using the indirect laser-induced temperature jump technique. Analysis of the distance dependence indicates that, unlike other bridges studied to date, the rate constants are not limited by electronic coupling for bridges up to 28 angstroms long. The energy levels of the bridges relative to those of the redox species rule out hopping through the bridge. We conclude that, out to 28 angstroms, the transfer is limited by structural reorganization and that electron tunneling occurs in less than 20 picoseconds, suggesting that oligophenylenevinylene bridges could be useful for wiring molecular electronic elements.

The development of novel electronic devices based on molecular materials such as organic light-emitting diodes (*1*, *2*), biosensors (*3*), and molecular electronic devices (*4*) is focusing interest on electron transfer across interfaces between conventional electrodes and molecular materials and, specifically, on the promotion of fast electron transfer through molecular bridges over large distances. The distance dependences of rate constants reported thus far for long-distance electron-transfer reactions involving a single electron tunneling step are well described by the superexchange model (*5*, *6*) in which the electron-transfer rate constant, k_{et}, decreases exponentially with increasing distance, x, separating a donor-acceptor pair or an electrode and a redox species. The decay constant, commonly referred to as β ($= -d\ln[k_{et}]/dx$), depends strongly on the degree of quantum mechanical coupling between the donor and acceptor (or between the electrode and the redox species) through a bridge. Values of β are typically about 1.0 Å^{-1} for electron transfer through saturated bridges and 0.2 to 0.6 Å^{-1} for unsaturated bridges (*7*, *8*). In cases where the donor/acceptor levels are near the occupied or unoccupied bridge levels, electron transfer to or from the bridge is possible, and multistep, hopping mechanisms allow markedly decreased distance dependences (*9–11*).

In our effort to identify useful bridges for interconnecting molecular electronic elements by rapid electron tunneling over distances of several nanometers, we found that oligophenylenevinylene bridges provide very effective electron tunneling paths. The Arrhenius prefactors for electron transfer through bridge lengths greater than 15 Å are substantially greater than measured previously for oligophenyleneethynylene bridges (*7*, *12*), possibly because of greater coplanarity of the phenylene units. Oligophenylenevinylene bridges also show an unexpectedly low distance dependence of the prefactors out to 28 Å. We argue that the electronic coupling through bridges 28 Å or shorter is strong enough to effect tunneling so fast (<20 ps) that it does not limit the rate of electron transfer. We suggest that structural reorganization of the redox species with respect to the monolayer-water interface may be rate limiting below 28 Å.

We synthesized a series of ferrocene oligophenylenevinylene methyl thiols (Fig. 1) by a method described elsewhere (*13*). Self-assembled, mixed monolayers were deposited from chloroform solutions containing a ferrocene oligophenylenevinylene methyl thiol (0.03 to 0.09 mM) and a saturated alkane thiol as diluent (0.27 to 0.21 mM) (*13*). Cyclic voltammetry (Fig. 2) and ellipsometry indicate that the monolayers are densely packed and composed mostly of diluent molecules, with a minority component of nearly isolated and identical redox sites that are outside the charge double layer and not lying down close to the gold electrode.

Electron transfer through even the longest bridge was too fast to measure with cyclic voltammetric or chronoamperometric techniques at a macroelectrode. Instead, we probed the electron-transfer kinetics using the indirect laser-induced temperature jump (ILIT) technique (*14*, *15*), which we have previously used to measure interfacial electron-transfer rates for other ferrocene-terminated thiol monolayers on gold (*7*, *16*). A laser-induced temperature change perturbs the interfacial equilibrium and causes a measurable change $\Delta V(t)$ in the initial open-circuit interfacial potential E_i. Figure 3A shows $\Delta V(t)$ following the laser pulse when the potential was initially poised far from the formal potential, $E^{o'}$, of the surface-bound redox couple. Under these conditions, the electron transfer–induced magnitude of the relaxation is very small. The ILIT response is effectively the thermal response in the absence of electron transfer and is directly proportional to a dimensionless function $\Delta T^*(t)$, which is a convolution of the instrument response and the rapid increase and much slower decrease in the interfacial temperature (*14–16*).

Figure 3B shows the open-circuit response when the system was initially poised at the $E^{o'}$ of the redox couple. The change in the interfacial potential is now a convolution of the electron-transfer relaxation and the thermal response, $\Delta T^*(t)$. The measured rate constant of the electron-transfer relaxation, $k_m(E_i)$, was determined by a fit to Eq. 1 (*14–16*)

$$\Delta V(t) = A'\Delta T^*(t) + k_m(E_i)B'\int_0^t e^{-k_m(t-\tau)}\Delta T^*(\tau)d\tau \qquad (1)$$

where A' is the amplitude of the thermal response and B' is the amplitude of the electron-transfer relaxation. Standard electrochemical rate constants, k^o, were extracted from $k_m(E_i)$ data for a range of initial poise potentials by an established procedure (*17*) (Fig. 4).

Standard rate constants were measured in the temperature range of 4° to 25°C; Fig. 5 shows an example of an Arrhenius plot of the temperature dependence of k^o. Activation energies, E_a, and prefactors, A, were obtained by fitting these plots to Eq. 2

$$k^o = A\exp[-\frac{E_a}{RT}] \qquad (2)$$

where R is the ideal gas constant. Table 1

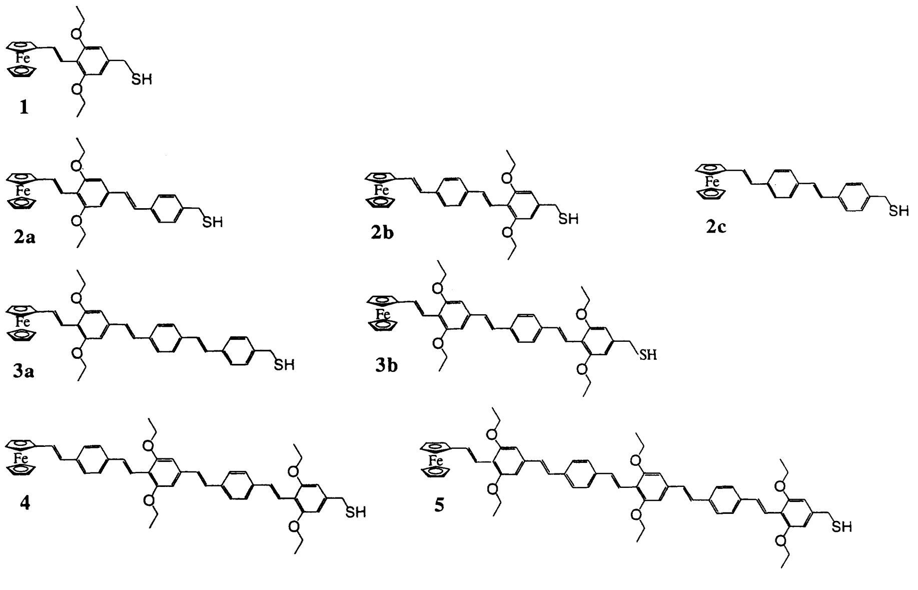

Fig. 1. Ferrocene oligophenylenevinylene methyl thiols (*13*).

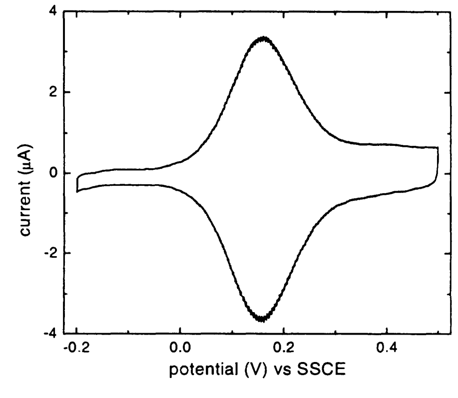

Fig. 2. Cyclic voltammogram of a mixed monolayer containing **3a** and decanethiol as diluent (sample 9 in Table 1). The scan rate was 100 mV/s. The symmetric ferrocene oxidation and ferrocenium reduction peaks have a formal potential of 162 mV versus SSCE and a fwhm of 108 mV, which is close to the theoretical value of 90 mV for isolated, noninteracting redox sites. Integration of the peaks above an interpolated baseline gives a ferrocene coverage of 4.4 × 10^{-11} mol/cm^2, corresponding to 11% of the total thiols on the surface.

---

[1]Department of Chemistry, Stanford University, Stanford, CA 94305–5080, USA. [2]Brookhaven National Laboratory, Upton, NY 11973, USA.

*To whom correspondence should be addressed. E-mail: smalley@bnl.gov, newton@bnl.gov, chidsey@stanford.edu, feldberg@bnl.gov

collects the values of k° ($T = 25°\mathrm{C}$), E_a, and A for different redox adsorbates, diluents, electrolytes, electrolyte concentrations, and coverages of ferrocene, N_T. The rate constant for electron transfer at 25°C through **1** is about 10 times greater than the nearly identical rate constants of about $3 \times 10^6\ \mathrm{s}^{-1}$ for electron transfer for molecules **2a, 2b, 2c, 3a, 3b**, and **4** (Fig. 1). However, **1** also has a smaller E_a for electron transfer than the other compounds, and thus the Arrhenius prefactors for **1** to **4** show only a weak distance dependence. The rate constant for **5** drops off somewhat and has a lower prefactor. For bridge lengths **1** to **4**, rate constants, activation energies, and prefactors are identical to within the experimental uncertainties for compounds with and without solubilizing groups (**2b** and **2c**), with different placement of solubilizing groups (**2a** and **2b**), and with different number of solubilizing groups (**3a** and **3b**). For comparison, k° ($T = 298$ K) was reported to be $6 \times 10^4\ \mathrm{s}^{-1}$ for a ferrocene-terminated oligophenyleneethynylene thiol with four repeat units (*12*), about 50 times smaller than the value for the oligophenylenevinylene tetramer reported here. Figure 6 is a plot of all of the prefactors from Table 1 as a function of bridge length (*18*). For bridge lengths out to 28 Å (after which the prefactor drops substantially), the slope obtained by linear regression of the natural log of the prefactors versus bridge length is $-0.06\ \text{Å}^{-1}$.

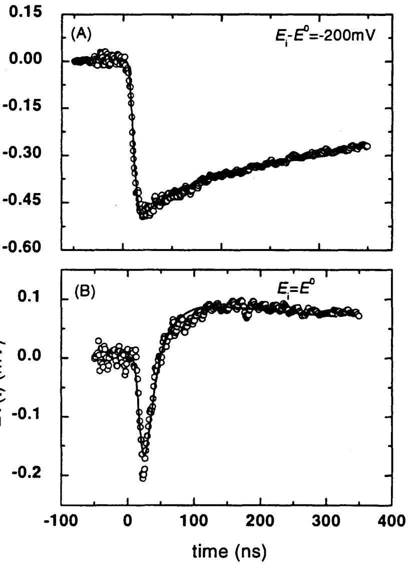

Fig. 3. Examples of ILIT transients (at 25°C) from sample 15 in Table 1. (**A**) $E_i - E^\circ = -200$ mV. (**B**) $E_i = E^\circ$. In the ILIT method, a gold film (~1 μm) electrode is vapor-deposited on a quartz disk after vapor deposition of a ~0.05-μm, light-absorbing adhesion layer of titanium. A laser pulse (λ_L = 1.06 μm; fwhm ≈ 10 ns) impinges on the titanium side of the electrode; the photoenergy is degraded within ~1 ps to heat that diffuses within a few nanoseconds to the interface between the monolayer-coated front of the electrode and an electrolyte solution.

We investigated and ruled out a number of possible artifacts in our measurement technique to ensure that we are not limited by the response time of the ILIT system (*19*). Uncompensated solution resistance is not a concern because the ILIT response is a change in the open-circuit potential, measured here with an amplifier with a high enough input impedance that a negligible current is passed through the solution. To confirm this claim, we changed the solution resistance by reducing the concentration of perchloric acid electrolyte from 1.0 to 0.1 M and saw no change in the resulting rate constant (see sample 11 in Table 1). The details of the experiment provide two internal confirmations that we are, in fact, measuring an electron-transfer relaxation. The measured rate constants, $k_m(E_i)$, are always well fit by the expected potential dependence (*17*) shown in Fig. 4, and the standard rate constants, k°, are always independent of N_T (see samples 3 and 4 in Table 1).

The distance dependence of the prefactors (Table 1 and Figure 6) for **1** to **4** is too weak to be consistent with an electron-transfer process limited by single-step electron tunneling (i.e., nonadiabatic electron transfer through a rigid bridge). A multistep hopping mechanism with electron transfer to and from the bridge rather than a single-step mechanism is another explanation for a weak dependence on bridge length. Such a mechanism has recently been confirmed for photoinduced, intramolecular electron transport through certain oligonucleotides (*9*, *11*) and was used to explain the weak distance dependence of some of the results for photoinduced electron transfer and its thermal back reaction through oligophenylenevinylenes between tetracene and pyromellitimide (*10*). However, this mechanism does not explain the present results. In contrast with the above cases, the energetics in our case are unfavorable for transfer of an electron or a hole between either the electrode or the ferrocene and the oligophenylenevinylene (*20*). The alternative is that the electron transfer is a single-step tunneling process through the bridge.

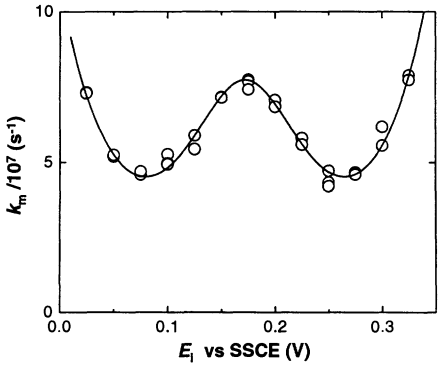

Fig. 4. k_m as a function of E_i (at 25°C) for sample 6 in Table 1. The solid curve is a fit to Eq. 19 in (*17*).

If this tunneling process were rate limiting, theory predicts (*8*, *21*), and numerous experiments (*6*–*8*, *12*, *16*) on widely varied systems have confirmed, that the rates should fall off exponentially with increasing bridge length. This exponential decay is a reflection of the exponential decay with distance of the square of the electronic matrix element, H_{ab}, which quantifies quantum mechanical coupling across the bridge. H_{ab} values in the model system ferrocene-vinylene(phenylenevinylene)$_n$-ferrocenium (n = 1 to 4) were obtained from semiempirical electronic structure calculations at the INDO/S (*22*) configuration interaction level, analyzed in terms of the Generalized Mulliken Hush method (*23*). The square of the resulting couplings decreased approximately exponentially with a distance dependence of $\beta \sim 0.4\ \text{Å}^{-1}$ (*24*). The observed distance dependence of 0.06 Å^{-1} for **1** to **4** is thus much weaker than the theoretical expectation based on the nonadiabatic model.

The weak distance dependence of our measured prefactors for **1** to **4** suggests that the quantum mechanical coupling between the electrode and ferrocene through the oligophenylenevinylene bridge is sufficiently strong (*25*) that electron transfer is limited by a process slower than electron tunneling; that is, the electron transfer is adiabatic. The decreased prefactor for **5** could signal the end of this adiabatic, weakly distance-dependent regime and the beginning of the regime in which the rate is limited by the distance-dependent coupling. We are in the process of synthesizing bridges with six and seven phenylenevinylene repeat units and suspect that we will find an exponential decrease of the rate with these longer bridge lengths.

The identity of the rate-limiting process in the case of **1** to **4** is not immediately obvious. It cannot be the formation of a structural intermediate before electron transfer because our rates show the expected potential dependence (*17*). Solvent reorientation about the

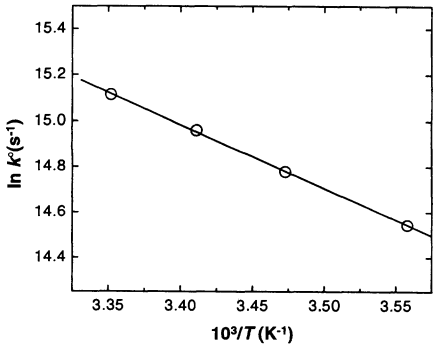

Fig. 5. Variation of the standard rate constant with temperature for sample 4 in Table 1.

Table 1. Summary of experimental data.

Sample	Compound*	Diluent	N_T (pmol/cm^2)	k^o (T = 298 K) ($\times 10^6$ s^{-1})	E_a (eV)	A ($\times 10^{10}$ s^{-1})
1	**1**	$HS(CH_2)_4CH_3$	7.7	45	0.203	12.4
2	**1**	$HS(CH_2)_4CH_3$	3.7	47	0.195	9.27
3	**2a**	$HS(CH_2)_9CH_3$	55	3.6	0.262	9.60
4	**2a**	$HS(CH_2)_9CH_3$	12	3.7	0.240	4.09
5	**2a**†	$HS(CH_2)_9CH_3$	41	3.6	0.252	6.47
6	**2b**	$HS(CH_2)_9CH_3$	26	3.6	0.253	6.90
7	**2c**	$HS(CH_2)_9CH_3$	82	3.6	0.256	7.58
8	**3a**	$HS(CH_2)_9CH_3$	37	3.7	0.255	7.75
9	**3a**	$HS(CH_2)_9CH_3$	44	3.6	0.242	4.30
10	**3a**	$HS(CH_2)_{11}CH_3$	42	3.7	0.241	4.30
11	**3a**‡	$HS(CH_2)_9CH_3$	27	3.7	0.239	3.89
12	**3a**§	$HS(CH_2)_9CH_3$	52	2.7	–§	–§
13	**3a**†	$HS(CH_2)_9CH_3$	32	3.7	0.245	5.04
14	**3b**	$HS(CH_2)_9CH_3$	41	3.7	0.249	5.94
15	**4**	$HS(CH_2)_{16}OH$	13	2.8	0.229	2.02
16	**4**	$HS(CH_2)_{16}OH$	20	2.8	0.245	3.89
17	**5**	$HS(CH_2)_{16}OH$	41	0.54	0.236	0.52
18	**5**	$HS(CH_2)_{15}CH_3$	11	0.55	0.251	0.97

*Structures shown in Fig. 1. Unless otherwise indicated, the electrolyte was 1.0 M $HClO_4$. †1.0 M H_2SO_4. ‡0.1 M $HClO_4$. §Experiment performed with the faster titanium-sapphire laser (*19*). The electrolyte was 1.0 M $NaClO_4$ and the temperature dependence of the rate constant was not studied.

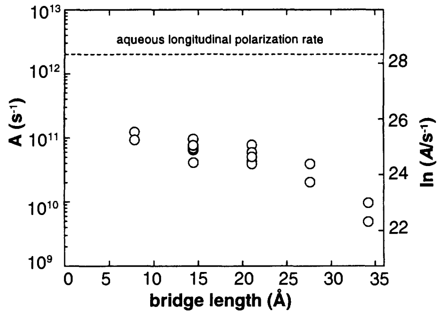

Fig. 6. Prefactors as a function of bridge length for all samples listed in Table 1. The dashed line shows the prefactor expected for an electron-transfer reaction limited by aqueous solvent dynamics.

neutral ferrocene and positively charged ferrocenium, which might be expected to be the rate-limiting process, cannot explain the prefactors observed. The time scale for solvent reorientation, known as the longitudinal relaxation time (*26*), is on the order of 0.5 ps for water (*27*), much faster than the reciprocals of our measured prefactors (10 to 30 ps). Two general types of explanations can be offered for these low prefactors. They may be due to negative activation entropy—a "tight" transition state—or due to unexpectedly slow reorganization accompanying electron transfer. Although we have no concrete suggestion for possible sources of a negative entropy of activation, we can make a suggestion for the cause of slower than expected reorganization. Translational diffusion on the molecular length scale leads to rates of the order of magnitude that we have observed. What might the translating species be? Perchlorate anions have been shown to ion pair with ferrocenium groups attached to an alkane thiol monolayer (*28*). However, because we have seen no dependence of the rate constant on the concentration or identity of the anion (see samples 4 versus 5 and 9 versus 11 versus 13 in Table 1), we conclude that the motion of the anion is not rate-limiting in our system.

Alternatively, the tethered redox species itself may translate. For instance, the hydrophobic, neutral ferrocene may be in contact with the hydrophobic methyl and methylene groups of the diluent monolayer and may diffuse into the water layer during oxidation to the positively charged ferrocenium. The diffusion constant of a small molecule in water is typically ~5 × 10^{-6}cm^2/s; therefore, ferrocene would move on the order of an angstrom in 20 ps, a distance consistent with that occupied by a layer of water molecules. We note, however, that changing the length and termination of the diluent does not markedly affect the rate, so the rate of diffusion from a hydrophobic to a hydrophilic environment would have to be independent of the exact structure of the interface. We intend to test this hypothesis by synthesizing bridges terminated with hydrophilic redox species, which will be fully solvated by water in both redox states.

We have shown that oligophenylenevinylene bridges can provide sufficient coupling to support electron transfer with an Arrhenius prefactor of ~1 × 10^{11} to ~3 × 10^{10} s^{-1} out to a bridge length of 28 Å. This level of coupling could be of use in interconnecting molecular electronic devices with little or no energy loss. However, for very fast operation, it will be important to understand the unexpected limitation of the adiabatic prefactors observed here.

References and Notes

1. C. W. Tang, S. A. Vanslyke, *Appl. Phys. Lett.* **51**, 913 (1987).
2. J. H. Burroughes *et al.*, *Nature* **347**, 539 (1990).
3. I. Willner, V. Heleg-Shabtai, R. Blonder, E. Katz, G. L. Tao, *J. Am. Chem. Soc.* **118**, 10321 (1996).
4. J. Chen, M. A. Reed, A. M. Rawlett, J. M. Tour, *Science* **286**, 1550 (1999).
5. H. M. McConnell, *J. Chem. Phys.* **35**, 508 (1961).
6. J. R. Miller, J. V. Beitz, *J. Chem. Phys.* **74**, 6746 (1981).
7. S. B. Sachs *et al.*, *J. Am. Chem. Soc.* **119**, 10563 (1997).
8. M. D. Newton, *Chem. Rev.* **91**, 767 (1991).
9. E. Meggers, M. E. Michel-Beyerle, B. Giese, *J. Am. Chem. Soc.* **120**, 12950 (1998).
10. W. B. Davis, W. A. Svec, M. A. Ratner, M. R. Wasielewski, *Nature* **396**, 60 (1998).
11. D. Porath, A. Bezryadin, S. deVries, C. Dekker, *Nature* **403**, 635 (2000).
12. S. Creager *et al.*, *J. Am. Chem. Soc.* **121**, 1059 (1999).
13. S. P. Dudek, H. D. Sikes, C. E. D. Chidsey, in preparation. Each compound was fully characterized by nuclear magnetic resonance (NMR), mass spectrometry, and elemental analysis. The NMR spectra are consistent with pure trans isomers. The relative orientations of the cyclopentadienyl rings and of the vinylenes about the aromatic rings are not known.
14. J. F. Smalley, C. V. Krishnan, M. Goldman, S. W. Feldberg, I. Ruzic, *J. Electroanal. Chem.* **248**, 255 (1988).
15. J. F. Smalley, L. Geng, S. W. Feldberg, L. C. Rogers, J. Leddy, *J. Electroanal. Chem.* **356**, 181 (1993).
16. J. F. Smalley *et al.*, *J. Phys. Chem.* **99**, 13141 (1995).
17. J. F. Smalley, M. D. Newton, S. W. Feldberg, *Electrochem. Commun.* **2**, 832 (2000).
18. For simplicity, we define the bridge length to be the length of the oligophenylenevinylene segment plus the length of a methylene unit (neglecting the thiol terminus). Use of standard bond lengths and angles gives a phenylenevinylene repeat length of 6.6 Å.
19. In the apparatus used to collect most of the kinetics data in Table 1, the response time of the detection system, including the laser pulse width, the amplifiers, and the oscilloscope, is ~10 ns. An experiment with improved instrumentation with a response time of ~1 ns resulted in a rate constant similar to that obtained with the usual, slower apparatus (see sample 12 in Table 1). This measurement used the titanium-sapphire laser [λ_L = 798 nm; full width at half-maximum (fwhm) ~100 fs] at Brookhaven National Laboratory's Laser Electron Accelerator Facility (LEAF).
20. The oxidation potential of the ferrocene is 0.17 V versus sodium-saturated calomel electrode (SSCE) and the electrode potentials for all our measurements are within 0.15 V of this value. The reported literature values (*10*) of the oxidation potentials of typical oligophenylenevinylenes range from 1.8 V (for one repeat unit) to 0.96 V (for four repeat units) versus SSCE. Thus, hole transfer from ferrocenium to oligophenylenevinylene is uphill by at least 0.8 eV. Similarly, on the basis of reported visible absorption spectra (*10*), electron transfer from ferrocene to oligophenylenevinylene is uphill by at least 1.6 eV. Because we observe activation energies of no more than 0.25 eV for the electron-transfer process, hopping through the bridge is ruled out. Dipole fields in the monolayer might displace the bridge levels with respect to the ferrocene. However, ion permeation into the monolayer is expected to make such dipole potentials negligible on the minutes time scale of the ILIT preequilibration. In fact, ion permeation into these monolayers is observed in cyclic voltammograms on the seconds time scale.
21. *Chem. Rev.* **92** (no. 3) (1992).
22. M. C. Zerner, G. H. Loew, R. F. Kirchner, U. T. Muellerwesterhoff, *J. Am. Chem. Soc.* **102**, 589 (1980).
23. R. J. Cave, M. D. Newton, *Chem. Phys. Lett.* **249**, 15 (1996).
24. Additional model calculations in which the ferrocene/ferrocenium groups were replaced by CH_2/CH_2^+ groups [as in (*7*)], either with or without methoxy substituent groups on some of the phenylene rings, yielded quite similar beta values.

25. The experimental rate constants and activation energies can be used to obtain a minimum H_{ab} value (*16*). With a density of states of 0.3 eV^{-1} per gold atom, a reorganization energy of 0.9 eV, and a rate constant of 3×10^6 s^{-1}, nonadiabatic electrochemical Marcus theory gives a minimum H_{ab} value of 52 cm^{-1} at 298 K. The calculated H_{ab} in the case of the $n = 4$ model compound was 2.6 cm^{-1}. Calculated H_{ab} values cannot be directly compared with experimental H_{ab} values because the model system has a ferrocene group where the experimental system has gold atoms. To account for this difference, we assume tight coupling between the bridge and one carbon atom of the ferrocene in the model system and tight coupling between the bridge and one gold atom in the experimental system. Additionally, we assume that the additional vinylene in the model system is equivalent to the methyl thiol in the experimental system. The quantum calculation gives a wave function amplitude on the ferrocenyl carbon of 0.14. Division of the calculated H_{ab} by this coefficient yields a more appropriate value of 18 cm^{-1} for comparison with the lower limit of the experimental H_{ab} value. This value is within a factor of 3 of the minimum obtained from experiment. Given the uncertainties in the calculation, we consider this result consistent with the conclusion that the rate is not limited by the electronic coupling.

26. L. D. Zusman, *Chem. Phys.* **49**, 295 (1980).

27. J. Barthel, K. Bachhuber, R. Buchner, H. Hetzenauer, *Chem. Phys. Lett.* **165**, 369 (1990). $\tau_L = (\varepsilon_\infty/\varepsilon_o)\tau_D$, where τ_L is the longitudinal polarization time, ε_∞ is the infinite-frequency dielectric constant, ε_o is the static dielectric constant, and τ_D is the Debye relaxation time.

28. G. K. Rowe, S. E. Creager, *Langmuir* **7**, 2307 (1991).

29. H.D.S. acknowledges an NSF Graduate Fellowship. S.P.D. acknowledges support from National Research Service Award 5 T32 GM08412 from the National Institute of General Medical Science. H.D.S., S.P.D., and C.E.D.C. acknowledge support from the NSF (CHE-9412720) and the Stanford Office of Technology Licensing. J.F.S., A.R.C., M.D.N., and S.W.F. acknowledge support from the Chemical Sciences Division, Department of Energy (DE-AC02-98CH10886).

13 September 2000; accepted 17 January 2001

Automated Solid-Phase Synthesis of Oligosaccharides

Obadiah J. Plante, Emma R. Palmacci, Peter H. Seeberger*

Traditionally, access to structurally defined complex carbohydrates has been very laborious. Although recent advancements in solid-phase synthesis have made the construction of complex oligosaccharides less tedious, a high level of technical expertise is still necessary to obtain the desired structures. We describe the automated chemical synthesis of several oligosaccharides on a solid-phase synthesizer. A branched dodecasaccharide was synthesized through the use of glycosyl phosphate building blocks and an octenediol functionalized resin. The target oligosaccharide was readily obtained after cleavage from the solid support. Access to certain complex oligosaccharides now has become feasible in a fashion much like the construction of oligopeptides and oligonucleotides.

The understanding of oligosaccharides and glycoconjugates in nature is still in its infancy (*1*). Cell surface glycoconjugates are involved in signal transduction pathways and cellular recognition processes and have been implicated in many disease states (*2*). A major impediment to the rapidly growing field of molecular glycobiology is the lack of pure, structurally defined carbohydrates and glycoconjugates. These biomolecules are often found in low concentrations and in microheterogeneous form in nature, greatly complicating their identification and isolation. The procurement of sufficient quantities of defined oligosaccharides required for detailed biophysical and biochemical studies therefore relies on efficient synthetic methods.

Although much progress has been made in oligosaccharide synthesis (*3*), the construction of complex carbohydrates remains time consuming and is carried out by a small number of specialized laboratories. The necessary functionalization of all hydroxyl groups present on a monosaccharide is one of the main challenges in oligosaccharide construction. The development of a protecting group scheme that allows for the manipulation of individual hydroxyl groups is pivotal for the success of the synthetic route. Permanent protecting groups, such as benzyl ethers, are installed at positions where a free hydroxyl will be present in the final deprotected molecule. Temporary protecting groups, such as esters, are used to mask hydroxyls that will be exposed at a certain stage of the synthesis. The liberated hydroxyl group then serves as a nucleophile in the reaction with a glycosylating agent.

The stereospecific formation of glycosidic bonds is the central challenge in carbohydrate chemistry (Fig. 1). The chemical formation of a glycosidic linkage involves activation of a glycosyl donor to create a reactive electrophilic species that couples with a nucleophilic acceptor hydroxyl. This coupling reaction can take two possible pathways resulting in formation of either α- or β-anomers. Current methods to control the stereochemistry of the anomeric center rely on the participation of a neighboring functionality, such as an ester-protecting group on the C2 hydroxyl. Formation of a cyclic oxonium ion intermediate shields one face of the molecule, leading exclusively to the formation of trans-glycosidic linkages. Cis-glycosidic bonds are difficult to construct with high specificity because neighboring group participation is not possible.

The evolution of a solid-phase paradigm for the construction of oligosaccharides was initiated with Frechet's synthesis of di- and trisaccharides on a polymer support in 1971 (*4*). Since then, solid-phase oligosaccharide synthesis has seen many advancements. Various glycosyl donors, such as anomeric sulfoxides (*5*) and anhydrosugars (*5*), have been applied to the synthesis of carbohydrates on a polymer support. Several linkers serving to connect the growing oligosaccharide chain to the polymer support have been introduced with different reactivities and cleavage procedures (*6*). Notably, a combinatorial split-and-mix approach on a support resulted in the synthesis of a library of *N*-acylated di- and trisaccharides (*7*). Although advancements in solid-phase chemistry have allowed for the construction of complex molecules, the manipulations remain tedious and time consuming.

Ultimately, a general, automated method for oligosaccharide assembly will allow for the rapid preparation of structures of interest. Oligonucleotides (*8*) and oligopeptides (*9*) are now routinely prepared in an efficient manner on automated synthesizers with solid-phase strategies. The solid-phase paradigm lends itself particularly well to automation of oligosaccharide synthesis as the repetitive nature of glycosylation and deprotection can easily be framed into a coupling cycle. Excess reagents can be used to drive reactions to completion, and resin washes can remove any soluble impurities. Only a single purification step is necessary after the sugar is liberated from the solid support.

Mindful of the advantages of solid-support synthesis, we considered several key issues for the development of an automated oligosaccharide synthesizer: (i) an instrument capable of performing repetitive chemical manipulations at variable temperatures, (ii) the design of an overall synthetic strategy with either the reducing or the nonreducing end of the growing carbohydrate chain attached to the support (*10*), (iii) selection of a polymer and linker that are inert to all reaction conditions during the synthesis but cleaved efficiently when desired, (iv) protecting group strategies consistent with the complexity of the target oligosaccharide, and (v)

Department of Chemistry, Massachusetts Institute of Technology, Cambridge, MA 02139, USA.

*To whom correspondence should be addressed. E-mail: seeberg@mit.edu